

**Accurate myocardial T₁ mapping at 5T using an improved MOLLI method:
A validation study**

Linqi Ge^{1,2#}, Yinuo Zhao^{1,2#}, Yubo Guo^{3#}, Yuanyuan Liu¹, Yihang Zhou¹, Haifeng Wang¹, Dong Liang¹, Hairong Zheng¹, Yining Wang³, Yanjie Zhu¹

¹Shenzhen Institutes of Advanced Technology, Chinese Academy of Sciences, 1068 Xueyuan Avenue, Guangdong, Shenzhen, China

²University of Chinese Academy of Sciences, 80 Zhongguancun East Road, Beijing, China

³Department of Radiology, State Key Laboratory of Complex Severe and Rare Diseases, Peking Union Medical College Hospital, Chinese Academy of Medical Sciences and Peking Union Medical College, Beijing, China

#Co-first authors: Linqi Ge, Yinuo Zhao, Yubo Guo

***Co-correspondence authors:**

Yanjie Zhu, Paul C. Lauterbur Research Center for Biomedical Imaging, Shenzhen Institutes of Advanced Technology, Chinese Academy of Sciences, Shenzhen, China; Tel: +86 0755 86392259; E-mail: yj.zhu@siat.ac.cn

Yining Wang, Department of Radiology, Peking Union Medical College Hospital, No.1, Shuaifuyuan, Dongcheng District, Beijing 100730, China; Tel: +86 136 6100 3076; E-mail: wangyining@pumch.cn

ABSTRACT

Purpose: To develop Coefficient-based Fitting with Adjustment (COFIA), which corrects both inversion efficiency and signal disturbance using empirically estimated factors, an improved 5T myocardial T_1 mapping method based on Modified Look-Locker Inversion Recovery (MOLLI), which addresses limitations in inversion factor, readout perturbations, and imperfect magnetization recovery.

Methods: The proposed COFIA method is based on a modified 5-(3)-3 MOLLI sequence with electrocardiogram (ECG) gating and gradient recalled echo (GRE) readout. To improve inversion factor at 5T, the inversion pulse was redesigned using adiabatic hyperbolic secant (HSn) and tangent/hyperbolic tangent (Tan/Tanh) pulses. Signal evolution was modeled recursively with inversion factor (δ) and a correction factor (C) to correct inversion imperfections, and T_1 values were estimated via nonlinear optimization. The method was validated in phantom studies, as well as in 21 healthy volunteers and 9 patients at 5T.

Results: The optimized inversion pulse based on the Tan/Tanh pulse was found to outperform the conventional HSn inversion pulse within a limited peak amplitude of 10.6 μT at the 5T scanner. This optimized inversion pulse achieves an average δ of 0.9014 within a ΔB_0 range of ± 250 Hz and a B_1 range of 225 to 540 kHz. Phantom studies show that the COFIA achieved high accuracy with errors within 5%. In vivo studies with 21 healthy volunteers, the native myocardial T_1 values were 1468 ± 48 ms (apex), 1514 ± 39 ms (middle), and 1545 ± 50 ms (base). The T_1 values of blood pool were 2182 ± 132 ms (apex), 2124 ± 153 ms (middle), and 2131 ± 158 m (base).

Conclusion: The proposed COFIA method demonstrated high accuracy in phantom studies and feasibility in vivo studies. By adopting the widely used 5(3)3 MOLLI acquisition scheme, it shows strong potential for clinical cardiac imaging at 5T.

Keywords: Myocardial T_1 mapping, 5T, improved MOLLI, COFIA

Abbreviations:

BPM	beats per minute
bSSFP	balanced steady state free precession
ECG	electrocardiogram
ECV	extracellular volume fraction
FOV	field-of-view
FSE	fast spin echo
GRAPPA	generalized autocalibrating partially parallel acquisition
GRE	gradient recalled echo
IR	inversion recovery
LGE	late gadolinium enhancement
MOLLI	MOdified Look Locker Inversion recovery
MR	magnetic resonance
MRI	magnetic resonance imaging
RF	radiofrequency
ROI	region-of-interest
SAPPHIRE	saturation pulse prepared heart rate independent inversion recovery
SAR	specific absorption rate
SASHA	saturation recovery single-shot acquisition
ShMOLLI	Shortened modified Look Locker inversion recovery
SNR	signal-to-noise ratio
T	Tesla
TE	echo time
TI	inversion time
TR	repetition time
MATLAB	MathWorks, Inc., Natick, Massachusetts, USA

1. Introduction

In the past few years, magnetic resonance myocardial T_1 mapping has become an essential tool for the direct quantification of myocardial tissue characteristic [1]. Compared to late gadolinium enhancement (LGE) [2], myocardial T_1 mapping as well as its derived parameter, extracellular volume (ECV) [3] demonstrates superiority in evaluating the degree of extracellular matrix expansion and delivers more accurate results in diffuse myocardial fibrosis detection [4]. In recent years, the advancement of high field whole-body MRI systems exceeding 3T, i.e., the 5T system, has gathered significant attention in cardiac imaging due to its improved signal-to-noise ratio (SNR) [5]. However, accurate myocardial T_1 mapping at 5T remains a technical challenge, requiring further development for robust clinical use.

Several techniques have been developed for myocardial T_1 mapping at 3T and 1.5T MR systems. The most popular technique is the Modified Look-Locker Inversion Recovery (MOLLI) method [6]. It acquires a series of T_1 -weighted images at different inversion times following an inversion pulse, obtaining the pixel-wise T_1 relaxation times by fitting the signal recovery curve to a three-parameter model. However, MOLLI requires data acquisition over multiple heartbeats, making the derived T_1 values susceptible to variations in heart rate. To address these issues, saturation recovery single-shot acquisition (SASHA) [7] replaces inversion recovery (IRs) with saturation pulses to eliminate heart rate dependence, yet its smaller dynamic signal range during recovery leads to a reduced SNR in obtained images as well as the derived T_1 maps. This drawback becomes even worse at 5T due to the longer T_1 values. Saturation pulse prepared heart rate independent inversion recovery (SAPPHIRE) [8] improves accuracy for long T_1 values by integrating inversion and saturation recovery, though its complexity limits clinical applications. The slice-interleaved T_1 (STONE) sequence [9] provides accurate T_1 mapping with high SNR, yet requires simultaneous acquisition of multiple slices. Model-based T_1 mapping [10] uses continuous acquisition via radial trajectories after a single inversion pulse, and then reconstructs T_1 maps directly from the acquired k-space data using a joint sparsity constrained model. This approach is resistant to motion artifacts, but its complex reconstruction process limits its clinical applicability.

Considering all trade-offs among the above techniques, we selected MOLLI-based method as the baseline method. MOLLI remains the most widely adopted clinical technique for myocardial T_1 mapping due to its robustness and reliability. However, its assumptions do not hold at 5T, where several key factors contribute to T_1 inaccuracy, as outlined below. (1) the inversion process is not always perfect. (2) MOLLI assumes full recovery between pulses, which is hard to achieve in tissues with prolonged T_1 at 5T or high heart rates. (3) MOLLI utilizes a fitting model initially developed for continuous GRE readouts [10], which leads to errors dependent on tissue T_1 and T_2 properties.

In this work, we aim to develop an accurate and clinically applicable myocardial T_1 mapping technique for 5T system, dubbed Coefficient-based Fitting with Adjustment (COFIA), which corrects both inversion efficiency and signal disturbance using empirically estimated factors and validate its performance in a multi-center study. Specifically, image acquisition is performed using a 5-(3)-3 MOLLI sequence with GRE readout, while the inversion pulse is redesigned using adiabatic hyperbolic secant (HSn) and tangent/hyperbolic tangent (Tan/Tanh) pulses to improve inversion factor at 5T. Then, the T_1 map is estimated using a scan specific fitting model, similar to the Instantaneous Signal Loss Simulation (InSiL) [11] approach, which involves the effects of inversion efficiency, readout gradients, and the subject's heart rate. The proposed method was first validated via a phantom study, and then evaluated in two imaging centers, including 21 healthy volunteers and 9 patients with cardiac diseases. Results demonstrate that our technique achieves high accuracy and is feasible for myocardial T_1 mapping at 5T system.

2. Methods

2.1 Sequence

The COFIA sequence was implemented on a 5T scanner (Jupiter, United Imaging Healthcare, China). The timing diagram of the sequence is shown in Figure 1. It uses a 5-(3)-3 MOLLI scheme consisting of two consecutive ECG-gated inversion recovery modified Look-Locker sequences. A 3-heartbeat rest period is introduced between two inversion pulses to allow recovery of longitudinal magnetization before the next inversion. Data acquisition is performed using GRE readout in the middle-diastolic cardiac phases, synchronized via ECG-gating. We

use GRE readout instead of the commonly used balanced steady state free precession (bSSFP), as bSSFP is prone to dark banding artifacts and has high specific absorption rate (SAR), making it less suitable for scanners with main magnetic field strengths above 3T.

2.2 T₁ fitting

To address the imperfections in the inversion process, the signal evolution is expressed as follows:

(1) The magnetization after the inversion pulse is given by:

$$M_{inv}(k)^+ = -\delta \cdot M_{inv}(k) \quad (1)$$

Where $M_{inv}(k)$ and $M_{inv}(k)^+$ denote the longitudinal magnetization right before and after the inversion pulse. The inversion factor δ accounts for the efficiency of the inversion pulse, and $k = 1, 2$ denotes the inversion index. The initial signal $M(1)_{inv} = M_0$ represents the equilibrium longitudinal magnetization, and $M(1)_{inv}^+ = -\delta \cdot M_0$.

(2) We hypothesize that disturbances caused by readouts are instantaneous and parameterized by a correction factor C ($0 < C < 1$):

$$M(j)_{ro}^+ = (1 - C) \cdot M(j)_{ro} \quad (2)$$

Here, $j = 1, 2, \dots, 5$ and $j = 6, 7, 8$ denotes the readout events after the first and second inversion pulse separately, which is consistent with our deliberately designed 5-(3)-3 MOLLI sequence. The subscript "ro" indicates readout events. $M(j)_{ro}$ and $M(j)_{ro}^+$ represent the signal immediately before and after the j -th single-shot acquisition, respectively.

(3) Based on the above principles, the longitudinal magnetization evolution can be described through a series of relaxation equations. In particular, the first acquisition process is expressed as follows:

$$M(1)_{ro} = M_0 + [M_{inv}(1)^+ - M_0] \exp\left(-\frac{\Delta T_1}{T_1}\right) \quad (3)$$

$$M(1)_{ro}^+ = (1 - C)M_0 \left[1 - [\delta + 1] \exp\left(-\frac{\Delta T_1}{T_1}\right)\right] \quad (4)$$

Where $M(1)_{ro}$ and $M(1)_{ro}^+$ represent the signal right before and after the first acquisition. ΔT_1 denotes the time interval between the first inversion pulse and the acquisition of k-space center line in the first readout. The signal at subsequent acquisition steps can be computed recursively as the following formulation:

$$M(i)_{all} = M_0 + [M(i-1)_{all}^+ - M_0] \exp\left(-\frac{\Delta T_i}{T_1}\right) \quad (5)$$

Here, $i = 1, 2, \dots, 10$ denotes either the inversion event or readout event, where ΔT_k denotes the time interval between an inversion pulse and the subsequent imaging acquisition, or between two consecutive imaging acquisitions.

(4) According to the above equations, the MR signals at all timepoints can be simulated, which contain four unknowns M_0 , T_1 , δ , and C . These unknowns can be estimated by minimizing the mean squared errors between the simulated and measured signals [12]. To reduce computational complexity and improve fitting robustness, the inversion factor δ is pre-calculated using a pre-scan, as described below. Then a three-parameter nonlinear optimization equation is employed to estimate the remaining unknowns M_0 , T_1 , and C for each pixel as:

$$[M_0, T_1, C] = \underset{\{M_0, T_1, C\}}{\operatorname{argmin}} \left\{ \sum_{j=1}^J (M(j)_{ro} - S(j))^2 \right\}, \quad \text{where } J = 8 \quad (6)$$

Where $S(j)$ represents the actual measured signal, and $M(j)_{ro}$ represents the simulated signal. In this study, the Levenberg-Marquardt algorithm [13] is used to solve the optimization problem of Eq.(6).

2.3 Optimization of Inversion Pulse

The inversion factor δ is essential for accurate myocardial T_1 mapping [14]. Due to the SAR limitation at 5T, the maximum achievable B_1 value is 10.6 μ T (about 450kHz), which is much lower than the B_1 strength of the optimal adiabatic inversion pulse for myocardial T_1 mapping at 3T [14]. Therefore, the inversion pulse at 5T needs to be redesigned to optimize the inversion factor.

Two adiabatic inversion pulse designs considered in this study were HSn [15-18] and Tan/Tanh [16,17,19]. For HSn design, the formula is as follows:

$$\begin{cases} \omega_1(t) = B_1 \operatorname{sech}(\beta(2t/T_p - 1)^n) \\ \Delta\omega(t) = A \tanh(\beta(2t/T_p - 1)^n) \end{cases} \quad (0 < t \leq T_p), \quad (8)$$

where T_p is the duration of the pulses, A is the amplitude of the frequency sweep, and β and n are pulse shape parameters. The parameter ranges were: $n = 1, 2, 4$, and 8 , $A=100$ -1500Hz in 100Hz step, and $\beta = \operatorname{asech}(x)$ with $x = 0.005$ -0.02 in steps of 0.005. For Tan/Tanh design, the formula is as follows:

$$\begin{cases} \omega_1(t) = B_1 \tanh(2\xi t/T_p) \\ \Delta\omega(t) = A(\tan(\kappa(2t/T_p - 1))/\tan(\kappa)) \end{cases} \quad (0 < t \leq T_p), \quad (9)$$

where ξ and κ are pulse shape parameters. The parameter ranges of Tan/Tanh were: $A = 4000\text{-}15000\text{Hz}$ in 500Hz step, $\tan(\kappa) = 8$ to 30 in steps of 2 , and $\xi = 2$ to 20 in steps of 2 . The ranges and steps of the RF parameters were determined based on previous studies [14,20]. B_1 field strength was set to the maximum achievable value of 450kHz for all designs. Considering the limits on SAR and achievable B_1 , we empirically set the RF duration (T_p) range from 8 to 30 ms in 1 ms increments for both HSn and Tan/Tanh. To determine B_1 and B_0 variations at 5T , B_1 and B_0 field maps were acquired in the short-axis view using a small cohort of five volunteers using a 5T scanner. Based on the observed variations over the heart, the B_0 range was set from -250 Hz to 250 Hz for pulse optimization. The B_1 range was set as -50% to 20% relative to the nominal value. As the used B_1 was 450kHz , the corresponding B_1 range was $225\text{-}540$ kHz for pulse optimization.

The δ for a variety of inversion pulse designs were calculated using the Bloch simulation with $T_1 = 1500$ ms and $T_2 = 40$ ms. The simulation was conducted with the mri-rf package in the Michigan Image Reconstruction Toolbox (MIRT) [21]. The equilibrium magnetization M_0 was set to 1 , and δ was calculated as the ratio of the simulated longitudinal magnetization after the inversion pulse to M_0 . The δ across the B_0 and B_1 imperfection ranges were averaged and the pulse parameter combination with the highest average δ was identified as the optimized set of parameters.

2.4 Inversion factor estimation

In previous studies, the “MOLLI + M_0 ” sequence was proposed to estimate the inversion factor δ by acquiring an additional proton density-weighted (PD) image after the MOLLI readouts [6]. However, at 5T , such inline acquisition introduces a longer scan duration and extended breath-hold, especially in the presence of prolonged T_1 values. Therefore, in this study, we employed a separate sequence to estimate δ .

The timing diagram of this sequence is shown in Figure 2. It first acquires a PD-weighted image (I_0) using a single-shot GRE readout. After 5 -heartbeat interval to allow full recovery, an inversion pulse is applied, immediately followed by a second acquisition (I_{IR}). Myocardial

regions were manually delineated on both images, and the average signal within each region-of-interest (ROI) was calculated. Then δ was measured as the ratio of average myocardial signals of I_{IR} and I_0 . δ was measured in 21 healthy volunteers, and the mean value (0.855) was used for all T_1 fitting in Eq.(6).

2.5 Phantom study

All imaging experiments were conducted using 5T MR scanners (Jupiter, United Imaging Healthcare, China). Phantom study was performed to assess the precision of T_1 measurements using the proposed method. The phantom comprises 9 vials, which were made by NiCl₂-doped agarose gel with varying concentrations to mimic different cardiac compartments [22]. The T_1 values of the phantom were first measured using the IR-FSE sequence with a local transmit and 48-channel receiver head coil. The imaging parameters of the IR-FSE sequence were: TR/TE = 15s/9.56ms, FOV = 320×320 mm, slice thickness = 5 mm, bandwidth = 260 Hz/pixel, acquisition matrix = 320×256 mm and inversion times (TIs) = 75ms, 100ms, 125ms, 150ms, 200ms, 300ms, 500ms, 800ms, 1000ms, 1500ms, 2000ms, 2500ms. The T_1 values were fitted with a three-parameter model from images obtained using the IR-FSE sequence and served as the gold standard.

The imaging parameters of COFIA were: TR/TE = 4.35ms/1.59ms, FOV = 150×150 mm, acquisition matrix = 128×128 mm, slice thickness = 8 mm, flip angle = 7°, bandwidth = 800 Hz/pixel, and TIs = 155ms and 235ms. Image acceleration was performed using Generalized Autocalibrating Partially Parallel Acquisition (GRAPPA) with an acceleration factor R = 2 and 24 calibration lines. The simulated heart rate was 75 bpm. Accuracy was defined as the relative error (%) between the T_1 values measured by COFIA and those obtained using the IR-FSE [23]. Precision is defined as the standard deviation (SD) of the T_1 values obtained by COFIA within a ROI [23,24]. Agreement between the two methods was further assessed using a Bland–Altman analysis.

2.6 In-vivo study

The in-vivo study was performed in two centers: United Imaging Healthcare and Peking Union Medical College Hospital. The experiments were approved by the Institutional Review Boards (IRBs) of both centers, and informed consent was obtained from each participant before the

scan. A total of 21 healthy volunteers (12 males and 9 females, aged 34 ± 26 years) and 9 patients with cardiac diseases (5 males and 4 females, aged 46 ± 31 years) were recruited.

Healthy volunteers were recruited from both centers: 7 from United Imaging Healthcare and 14 from Peking Union Medical College Hospital. Inclusion criteria for healthy subjects included no history or symptoms suggestive of cardiovascular disease and no contraindications to MRI. Patients were recruited exclusively from Peking Union Medical College Hospital. Inclusion criteria for patients included referral for clinical CMR imaging due to suspected or confirmed cardiovascular disease. All patients were required to be able to comply with breath-holding instructions during image acquisition. The specific cardiomyopathies of these patients are summarized in Table 1.

For healthy volunteers, native T_1 maps were acquired for 3 short-axis slices, specifically the apex, middle, and base slices. For patients, both native and post Gd infusion T_1 maps were acquired from the same three short-axis slices. Imaging parameters were: TR/TE = 3.99ms/1.453ms, FOV = 256×228 mm, slice thickness = 8 mm, flip angle = 7°, bandwidth = 800 Hz/pixel, acquisition matrix = 256×148 mm, and TI = 155ms and 235ms. The acquisition window of each image was 295 ms. A 24-channel phased-array coil was used for signal reception. All T_1 -weighted images were first registered using a symmetric diffeomorphic registration algorithm [25] implemented on the scanner, and then fitted pixel-wise using Eq.(6) to obtain the T_1 map.

For the in-vivo analysis, the endocardial and epicardial borders of the left ventricle were manually delineated on the T_1 maps. The mean myocardial T_1 value for each short-axis slice was then calculated. In addition to myocardial T_1 , blood T_1 values were also measured. Sex-based comparisons of T_1 values among healthy volunteers were performed using independent samples t-tests for each slice. All analyses were conducted using MATLAB (R2023a, MathWorks, Natick, MA, USA).

3. Results

3.1 Simulations

The best HS_n design is achieved with $\beta = 0.02$, $A = 0.5$ kHz, power = 2, and $T_p = 10$ ms and the average $\delta = 0.8916$ over B_0 of ± 250 Hz and B_1 of -50% to 20% for B_1 , while the

parameters for the best Tan/Tanh design are $A = 10$ kHz, $K_s = 4$, $k = 22$, and $T_p = 8$ ms with an average $\delta = 0.9014$. The δ versus B_1 and off-resonance are graphed in Figure 3 for the best designs of both HSn and Tan/Tanh. The Tan/Tanh design exhibits higher inversion over a larger B_0 and off-resonance area than the HSn design. Additionally, the inversion pulse using the Tan/Tanh design exhibits a broad transitional band, which is advantageous for maintaining the uniformity of the blood pool. Therefore, we employed the Tan/Tanh design in this study.

3.2 Phantom study

Table 2 summarizes the T_1 values obtained using IR-FSE and COFIA across nine phantom tubes, along with the corresponding accuracy and precision of COFIA. The T_1 estimates from COFIA demonstrate high accuracy, with relative errors of less than 5% compared to IR-FSE. The precision of COFIA varies with the values of each tube. A Bland–Altman analysis was conducted to assess the agreement between COFIA and the reference IR-FSE method in terms of relative error. The mean relative bias was -0.72% , with 95% limits of agreement ranging from -5.89% to $+4.45\%$. All relative errors fell within $\pm 5\%$ across the T_1 range (350–2300 ms), indicating good consistency between the two methods (as shown in Figure 4).

3.3 In-vivo studies

The myocardial T_1 maps were fitted using $\delta = 0.855$. Figure 5 shows the T_1 maps at three short-axis in three healthy volunteers using COFIA and Supporting Information Figure S1 shows the corresponding C maps obtained after fitting. Figure 6 presents the native and post Gd infusion T_1 maps, as well as the corresponding T_1 -weighted images from three patients using the COFIA sequence. The average native myocardial T_1 values across 21 healthy volunteers were 1468 ± 48 ms, 1514 ± 39 ms, and 1545 ± 50 ms for apex, middle, and base slices, respectively. The T_1 values decrease progressively from the base to the apex. The T_1 values of blood pool were 2182 ± 132 ms, 2124 ± 153 ms, and 2131 ± 158 ms for apex, middle, and base.

A sex-based analysis revealed significantly higher T_1 values in males compared to females at the apex ($p = 0.002$) and middle ($p = 0.021$) slices among healthy volunteers, with no difference at the base ($p = 0.344$). These results are summarized in Table 3.

4. Discussion

This study presents the development and validation of a 5T myocardial T_1 mapping technique, the COFIA, which addresses the challenges associated with conventional MOLLI sequences at high field strengths. The proposed COFIA method achieved accurate and consistent T_1 estimation in phantom studies, showing good agreement with reference IR-FSE measurements. In vivo studies, the method produced stable myocardial T_1 maps across healthy volunteers and patients, with no significant differences observed between groups, supporting its potential clinical applicability at 5T.

Imperfect inversion pulses can introduce systematic errors in T_1 estimation. As reported in prior studies [26,27]. Achieving a high inversion efficiency is essential for accurate myocardial T_1 mapping, especially at high fields. Therefore, the inversion pulse was redesigned specifically for 5T conditions to improve the inversion efficiency. Furthermore, we observed that optimizing the adiabatic inversion pulse not only improves inversion efficiency but also enhances blood pool uniformity (see in Supporting Information Figure 2). At 5T, shimming is typically centered on the heart, resulting in reduced field homogeneity in inflowing blood. Using a broadband Tan/Tanh inversion pulse helps maintain uniform inversion across both local and distal blood pools, leading to more homogeneous T_1 maps.

In addition to the redesigned inversion pulse, the inversion efficiency was explicitly incorporated into the fitting model. In previous InSiL [11] and multiparametric SASHA (mSASHA) methods [28], the PD image is acquired by adding additional readouts to the imaging sequence, enabling pixel-wise estimation of the inversion factor. Although this strategy can be integrated in the proposed method, we opted to use a separate PD scan for two main reasons. First, the additional readout prolongs acquisition and breath-hold time, which may compromise patient compliance and image quality in clinical practice. Second, estimating inversion factor pixel-wise from inline PD images can lead to unstable fitting due to limited data points and increased model complexity (see in Supporting Information Figure S3). Using a separate PD scan enables more stable and efficient inversion factor estimation, facilitating a simplified and robust three-parameter fitting model. We acknowledge that inversion factor may vary between subjects and slices due to varying B_1 efficiency. Considering the tradeoff between stability and accuracy, we choose to use a fixed inversion factor estimated by the separate PD scan.

This study has several limitations. First, the sample size was relatively small, particularly in the patient group, and the type of disease for some patients is uncertain. This limited our ability to detect statistically significant differences in myocardial T_1 values between healthy volunteers and patients. Future studies with larger and more homogeneous patient cohorts will be necessary to further evaluate the clinical utility of the proposed method. Second, the use of GRE readouts, while beneficial for SAR, results in lower precision compared to bSSFP-based T_1 mapping, as reported in prior studies [29]. Although denoising filters can partially alleviate this limitation, additional work is needed to systematically improve precision. In future studies, we plan to investigate advanced fast imaging strategies, including deep learning-based methods, to enhance image quality and precision at 5T.

5. Conclusion

The proposed COFIA method demonstrated high accuracy in phantom studies and feasibility in vivo studies. By adopting the widely used 5(3)3 MOLLI acquisition scheme, it shows strong potential for clinical cardiac imaging at 5T.

Declarations

Ethics approval and consent to participate: The institutional ethics committee at Peking Union Medical College Hospital (Beijing, China) approved the study. All participants were required to provide written informed consent prior to recruitment.

Consent for publication: Written informed consent was obtained from all participants for inclusion of their data in publications.

Availability of data and materials: Anonymized datasets which include T₁ maps from healthy volunteers and patients, have been made publicly available via Zenodo (<https://doi.org/10.5281/zenodo.16417553>). All patient-identifiable information was removed and the sharing protocol was approved by the institutional review board.

Competing interests: The authors declare that they have no competing interests.

Funding: This study was supported by the National Natural Science Foundation of China (grants 62322119, 12226008, 82020108018, U22A20344) and Shenzhen Science and Technology Program (grants RCYX20210609104444089, JCYJ20220818101205012). Also supported by the Key Laboratory for Magnetic Resonance and Multimodality Imaging of Guangdong Province (grant 2023B1212060052).

Authors' contributions: All authors significantly contributed to this work, read and approved the final manuscript.

Acknowledgement: The authors would like to acknowledge United Imaging Healthcare for their valuable support in technical assistance, which greatly contributed to this research. And the authors thank each of the study subjects for their participation.

Author details: ¹Shenzhen Institutes of Advanced Technology, Chinese Academy of Sciences, 1068 Xueyuan Avenue, Guangdong, Shenzhen, China. ²University of Chinese Academy of Sciences, 80 Zhongguancun East Road, Beijing, China. ³Department of Radiology, State Key Laboratory of Complex Severe and Rare Diseases, Peking Union Medical College Hospital, Chinese Academy of Medical Sciences and Peking Union Medical College, Beijing, China

Reference

1. Taylor AJ, Salerno M, Dharmakumar R, Jerosch-Herold M. T1 mapping: basic techniques and clinical applications. *JACC: Cardiovascular Imaging*. 2016;9(1):67-81.
2. Messroghli DR, Moon JC, Ferreira VM, et al. Clinical recommendations for cardiovascular magnetic resonance mapping of T1, T2, T2* and extracellular volume: a consensus statement by the Society for Cardiovascular Magnetic Resonance (SCMR) endorsed by the European Association for Cardiovascular Imaging (EACVI). *Journal of Cardiovascular Magnetic Resonance*. 2016;19(1):75.
3. Haaf P, Garg P, Messroghli DR, Broadbent DA, Greenwood JP, Plein S. Cardiac T1 mapping and extracellular volume (ECV) in clinical practice: a comprehensive review. *Journal of Cardiovascular Magnetic Resonance*. 2016;18(1):89.
4. Tanigaki T, Kato S, Azuma M, Nitta M, Horita N, Utsunomiya D. Right ventricular myocardial fibrosis evaluated by extracellular volume fraction by magnetic resonance imaging in patients with repaired tetralogy of Fallot: a meta-analysis. *Heart and Vessels*. 2024;39(4):349-358.
5. Guo Y, Lin L, Zhao S, et al. Myocardial fibrosis assessment at 3-T versus 5-T myocardial late gadolinium enhancement MRI: early results. *Radiology*. 2024;313(2):e233424.
6. Messroghli DR, Radjenovic A, Kozerke S, Higgins DM, Sivananthan MU, Ridgway JP. Modified Look-Locker inversion recovery (MOLLI) for high-resolution T1 mapping of the heart. *Magnetic Resonance in Medicine: An Official Journal of the International Society for Magnetic Resonance in Medicine*. 2004;52(1):141-146.
7. Chow K, Flewitt JA, Green JD, Pagano JJ, Friedrich MG, Thompson RB. Saturation recovery single-shot acquisition (SASHA) for myocardial T1 mapping. *Magnetic resonance in medicine*. 2014;71(6):2082-2095.
8. Roujol S, Weingartner S, Foppa M, et al. Accuracy and reproducibility of four T1 mapping sequences: a head-to-head comparison of MOLLI, ShMOLLI, SASHA, and SAPPHERE. *Journal of Cardiovascular Magnetic Resonance*. 2014;16(Suppl 1):O26.
9. Weingärtner S, Roujol S, Akçakaya M, Basha TA, Nezafat R. Free-breathing multislice native myocardial T1 mapping using the slice-interleaved T1 (STONE) sequence. *Magnetic resonance in medicine*. 2015;74(1):115-124.
10. Wang X, Kohler F, Unterberg-Buchwald C, Lotz J, Frahm J, Uecker M. Model-based myocardial T1 mapping with sparsity constraints using single-shot inversion-recovery radial FLASH cardiovascular magnetic resonance. *Journal of cardiovascular magnetic resonance*. 2019;21(1):60.
11. Shao J, Nguyen KL, Natsuaki Y, Spottiswoode B, Hu P. Instantaneous signal loss simulation (InSiL): an improved algorithm for myocardial T1 mapping using the MOLLI sequence. *Journal of Magnetic Resonance Imaging*. 2015;41(3):721-729.
12. Khan NA, Qureshi MA, Akber S, Hameed T. Accrue ment of nonlinear dynamical system and its dynamics: electronics and cryptographic engineering. *Fractional Order Systems and Applications in Engineering*. Elsevier; 2023:133-156.
13. Wilamowski BM, Yu H. Improved computation for Levenberg–Marquardt training. *IEEE transactions on neural networks*. 2010;21(6):930-937.
14. Kellman P, Herzka DA, Hansen MS. Adiabatic inversion pulses for myocardial T1 mapping. *Magnetic resonance in medicine*. 2014;71(4):1428-1434.

15. Tannús A, Garwood M. Improved performance of frequency-swept pulses using offset-independent adiabaticity. *Journal of Magnetic Resonance*. 1996;120(1):133-137.
16. Tannús A, Garwood M. Adiabatic pulses. *NMR in Biomedicine: An International Journal Devoted to the Development and Application of Magnetic Resonance In Vivo*. 1997;10(8):423-434.
17. Garwood M, DelaBarre L. The return of the frequency sweep: designing adiabatic pulses for contemporary NMR. *Journal of magnetic resonance*. 2001;153(2):155-177.
18. Tesiram YA. Implementation equations for HS_n RF pulses. *Journal of Magnetic Resonance*. 2010;204(2):333-339.
19. Hwang T-L, Van Zijl PC, Garwood M. Fast broadband inversion by adiabatic pulses. Elsevier; 1998. p. 200-203.
20. Yang Y, Wang C, Liu Y, et al. A robust adiabatic constant amplitude spin-lock preparation module for myocardial T1 ρ quantification at 3 T. *NMR in Biomedicine*. 2023;36(2):e4830.
21. Fessler J. Michigan image reconstruction toolbox. 2018. URL: <https://web.eecs.umich.edu/~fessler/code>. 2018;
22. Captur G, Gatehouse P, Keenan KE, et al. A medical device-grade T1 and ECV phantom for global T1 mapping quality assurance—the T1 Mapping and ECV Standardization in cardiovascular magnetic resonance (TIMES) program. *Journal of cardiovascular magnetic resonance*. 2016;18(1):58.
23. Roujol S, Weingärtner S, Foppa M, et al. Accuracy, precision, and reproducibility of four T1 mapping sequences: a head-to-head comparison of MOLLI, ShMOLLI, SASHA, and SAPPHERE. *Radiology*. 2014;272(3):683-689.
24. Xu Z, Li W, Wang J, et al. Reference ranges of myocardial T1 and T2 mapping in healthy Chinese adults: a multicenter 3T cardiovascular magnetic resonance study. *Journal of Cardiovascular Magnetic Resonance*. 2023;25(1):64.
25. Avants BB, Epstein CL, Grossman M, Gee JC. Symmetric diffeomorphic image registration with cross-correlation: evaluating automated labeling of elderly and neurodegenerative brain. *Medical image analysis*. 2008;12(1):26-41.
26. Kellman P, Hansen MS. T1-mapping in the heart: accuracy and precision. *Journal of cardiovascular magnetic resonance*. 2014;16(1):2.
27. Rodgers CT, Piechnik SK, DelaBarre LJ, et al. Inversion recovery at 7 T in the human myocardium: measurement of T1, inversion efficiency and B1⁺. *Magnetic resonance in medicine*. 2013;70(4):1038-1046.
28. Chow K, Hayes G, Flewitt JA, et al. Improved accuracy and precision with three-parameter simultaneous myocardial T1 and T2 mapping using multiparametric SASHA. *Magnetic resonance in medicine*. 2022;87(6):2775-2791.
29. Jang J, Bellm S, Roujol S, et al. Comparison of spoiled gradient echo and steady-state free-precession imaging for native myocardial T1 mapping using the slice-interleaved T1 mapping (STONE) sequence. *NMR in Biomedicine*. 2016;29(10):1486-1496.

Tables

Table 1. The specific cardiomyopathies and myocardial T₁ values of patients.

ID	Diagnosis	Myocardium		Blood	
		Post Gd		Post Gd	
		Native T ₁ (ms)	infusion T ₁ (ms)	Native T ₁ (ms)	infusion T ₁ (ms)
P01	myocardial fat infiltration	1437	605	2234	404
P02	myocardial fat infiltration	1393	567	2419	437
P03	cardiac amyloidosis	1789	835	2012	672
P04	NICM	1615	634	2014	471
P05	NICM	1581	739	2174	457
P06	NICM	1496	696	2176	494
P07	NICM	1490	746	2032	453
P08	MINOCA	1509	722	2390	472
P09	MINOCA	1695	670	2443	401

NICM- non-ischemic cardiomyopathy, were not definitively diagnosed.

MINOCA- myocardial infarction with non-obstructive coronary arteries

Table 2. Native T₁ values, relative error and precision in nine tubes of IR-FSE and COFIA in phantom studies.

IR-FSE			COFIA		
No.	Reference T ₁ (ms)	δ	Native T ₁ (ms)	Relative Error(%)	Precision
1	599.6	0.896	582.5	2.85	5.67
2	1501.1	0.915	1498.3	0.19	22.40
3	654	0.954	646.7	1.12	7.14

4	788.9	0.873	767.6	2.70	9.01
5	1872.7	0.908	1860.9	0.63	28.70
6	2374	0.971	2260	4.80	40.31
7	440.9	0.882	435.2	1.29	5.05
8	1230.2	0.892	1270.5	3.28	17.62
9	357.3	0.941	371	3.83	3.45

Table 3. Sex-based comparison of native myocardial T₁ values (ms) in healthy volunteers.

Group	Slice	Male(Mean±SD)	Female(Mean±SD)	p-value
Healthy Volunteers	Apex	1495±30	1432±44	0.002
	Middle	1532±35	1489±30	0.021
	Base	1535±43	1557±58	0.344

Figure Legends

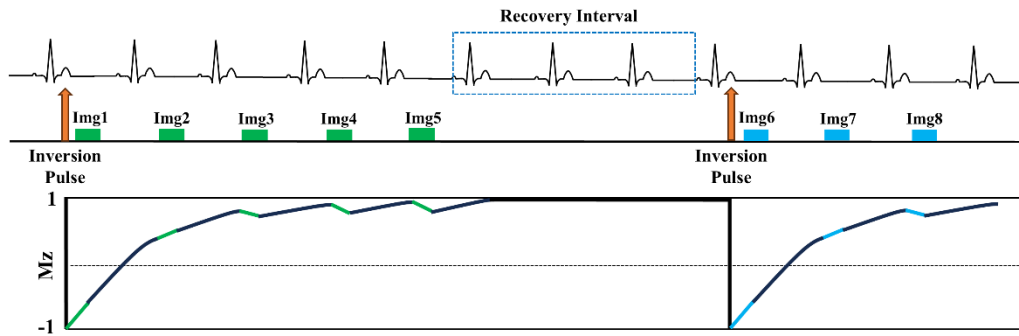


Fig 1. The timing diagram of the COFIA sequence. The acquisition scheme of the MOLLI sequence is 5(3)3. Initially, five images are acquired following the first inversion pulse, corresponding to five consecutive heartbeats during the diastolic period with intermittent image acquisition. A recovery interval of three heartbeats is allowed between the first and second inversion pulses to facilitate more complete T_1 recovery. After the second inversion pulse, three additional images are acquired.

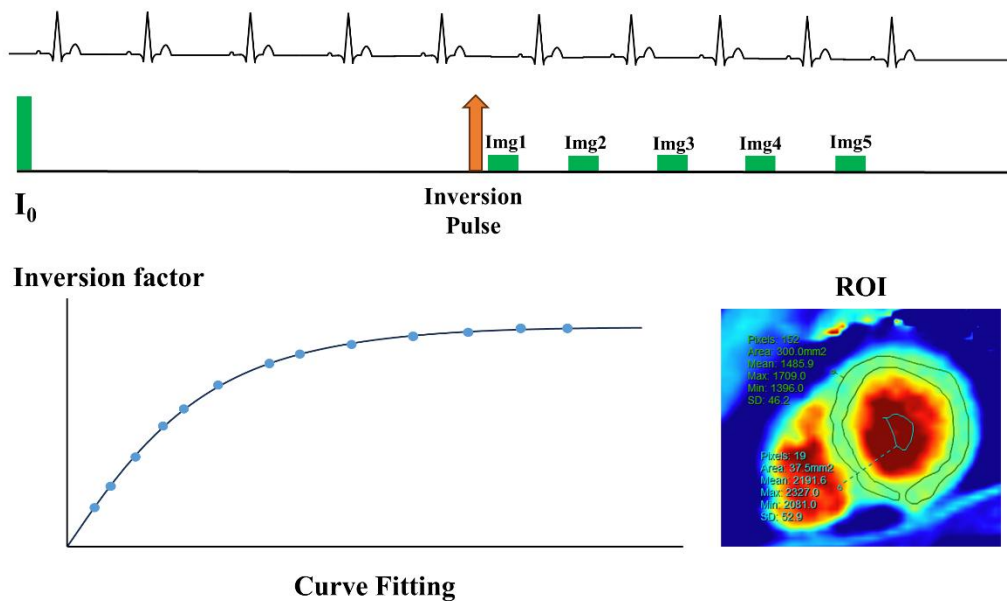


Fig 2. The timing diagram of the sequence for measuring inversion factor δ . Proton density images (I_0) are obtained using a single GRE acquisition. After 5 heartbeats, infrared pulses were applied immediately, followed by image acquisition. Sketched ROI to calculate δ , fitted the obtained values, and used the corrected inversion factor of 0.855 to fit the myocardial T_1 value.

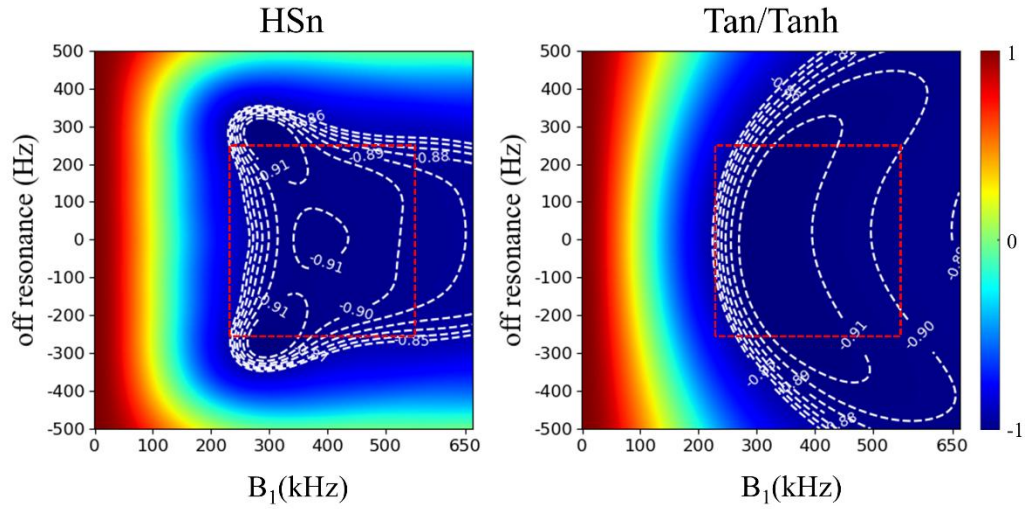


Fig 3. The δ maps of the best HSn and Tan/Tanh designs over a variety of B_0 and B_1 ranges (ΔB_0 : -250 to 250 Hz, B_1 : 225 to 540 kHz). The white dotted contours indicate isometric δ values, and the red dashed rectangles denote the desired B_0 and B_1 operating ranges.

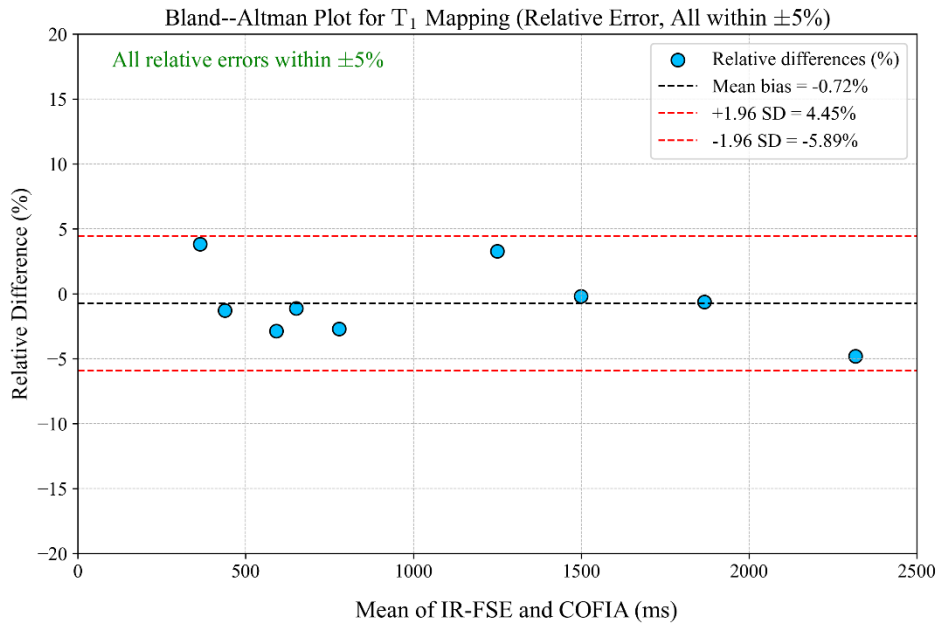


Fig 4. Bland–Altman plot comparing T_1 values measured by COFIA and IR-FSE in phantoms. Each blue dot represents the relative difference (%) plotted against the mean T_1 value of the two methods. The dashed black line indicates the mean bias (-0.72%), and the red dashed lines represent the 95% limits of agreement (-5.89% to $+4.45\%$).

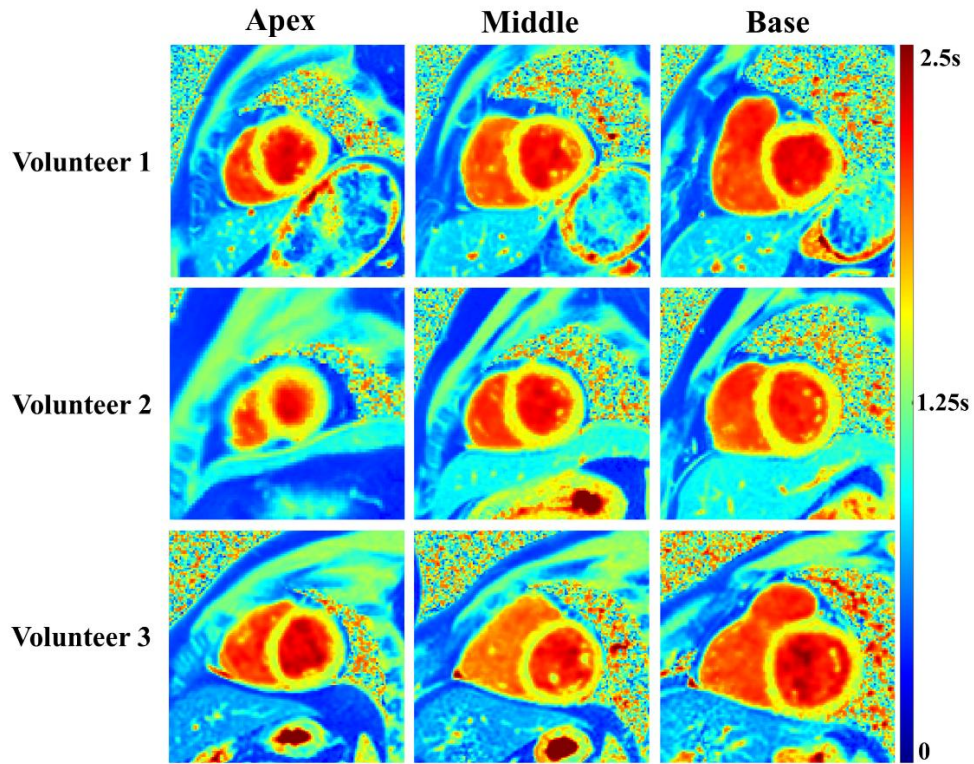


Fig 5. Native T_1 maps in three healthy volunteers at apex, middle, and base slices using COFIA.

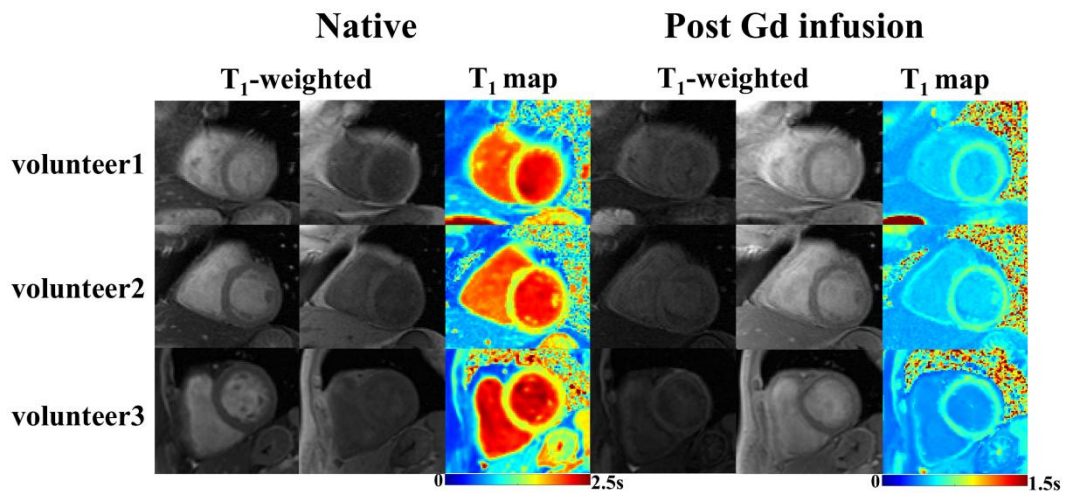


Fig 6. Representative native (left) and post Gd infusion (right) T_1 -weighted images and corresponding T_1 maps from 3 patients. The T_1 -weighted images show clear myocardial boundaries suitable for pixel-wise curve fitting.

Declaration of interests

The authors declare that they have no known competing financial interests or personal relationships that could have appeared to influence the work reported in this paper.